PHYSICAL REVIEW A VOLUME 22, NUMBER 3 SEPTEMBER 1980

Scaled proton ionization cross sections in the Born approximation

E. J. McGuire
Sandia Laboratories, Albuquerque, New Mexico 87185
(Received 6 August 1979)

Using the generalized oscillator strength formulation of the Born approximation, proton ionization cross sections were calculated for a large sample of subshells of atoms throughout the periodic table. The results are presented in the form of scaled cross sections for all subshells up to the $6p$. Comparison with measurements shows reasonable agreement (better than a factor of 2), with some exceptions, for the proton energy range studied. The scaled cross sections presented herein are limited, in general, to proton energies greater than 184 times the subshell ionization energy.

I. INTRODUCTION

The modeling of proton energy deposition in pellet fusion targets requires accurate (better than a factor of 2) stopping powers for ionized high-Z material. Nardi *et al.*[1] have shown that, at a temperature of 1 keV, energy deposition in the plasma dominates energy deposition in the bound electrons, and consequently a simple model for the latter energy deposition should suffice. Our concern is the physics at lower temperatures and, in particular, the role of excitation versus ionization in energy deposition in the bound electrons. Radiation from excited states could be a cooling mechanism inhibiting the achievement of high temperature. Hahn[2] has suggested that for high-Z materials the excitation cross section dominates the ionization cross section with increasing degree of ionization. It is not clear how this dominance is reflected in the stopping power.

Expressions for the stopping power of an arbitrary projectile incident in a target of arbitrary Z and temperature are available.[3] They are based on a judicious use of the Bethe formula[4] and experimental data. However, even when the extrapolation based on the Bethe formula and experimental data is reliable, there is no way to separate the contributions due to excitation and ionization. An alternative approach, adopted here, is to calculate the contribution of excitation and ionization of each atomic subshell to the stopping power, and determine subshell scaling laws. The calculations use the generalized oscillator strength formulation of the Born approximation (the starting point in the derivation of the Bethe formula). If scaling laws exist, then a reasonable sample of subshells and atoms should suffice to determine them. Calculations[5,6] of electron ionization cross sections for the entire periodic table have shown that such scaling laws do exist and can be determined with a reasonable sample of subshells. The generalized oscillator strengths (GOS) used in the electron ionization calculations were used to determine subshell proton ionization cross sections and stopping power due to ionization. The stopping power results will be reported later; here the scaled proton ionization cross sections are reported and compared with experiment. In the proton ionization calculations, the focus is on large subshell cross sections, that is, when the subshell ionization contributes significantly to the stopping power. The proton ionization cross section is small when the proton velocity is less than one-tenth the subshell orbital velocity, and, except for a brief discussion in Sec. III of the plateau region of the $2s$ cross section, low-velocity collisions are not treated.

In Sec. II, theory and assumptions in the calculation are summarized. In Sec. III the calculations are compared with measurements on Kr and Xe. In Sec. IV the scaled $1s$-, $2s$-, and $2p$-subshell cross sections are presented and compared with experiment, and some critical evaluations are made. In Sec. V the scaled $3s$, $3p$, and $3d$ cross sections are presented and the scaled $3d$ cross section is compared with experiment. In Sec. VI the scaled $4s$, $4p$, $4d$, and $4f$ cross sections are presented and the scaled $4d$ cross section is compared with two sets of measurements. In Sec. VII the scaled $5s$, $5p$, $5d$, $5f$, $6s$, and $6p$ cross sections are presented.

II. THEORY AND APPROXIMATIONS

The one-electron GOS to the continuum per nl electron per $\epsilon l'$ continuum hole is defined by

$$\frac{df_{nl}}{d\epsilon}(\epsilon, k^2, l') = \frac{\Delta E}{k^2} \left| \langle nl \left| e^{i\vec{k}\cdot\vec{r}} \right| \epsilon l' \rangle \right|^2 , \tag{1}$$

where $\Delta E = \epsilon - E_{nl}$ is in Ry (13.6 eV), $-E_{nl}$ is the one-electron ionization energy of the nl subshell, ϵ is the continuum electron energy, with $\epsilon = 0$ at the ionization threshold, r is in Bohr radii, k is in inverse Bohr radii, and df/de is in Ry^{-1}. Expanding the exponential in Eq. (1) in Legendre polynomials and Bessel functions leads to explicit ex-

pressions for subshell GOS involving one-electron orbitals. For $l=0,1,2$, the expressions are given in Ref. 7, while the $l=3$ expression is given in Ref. 8. The orbitals were generated via straight-line approximations to the quantity $[-rV(r)]$ of Herman and Skillman.[8] For $Z \leq 18$ four straight lines were used in the approximation, for $19 \leq Z \leq 36$ six straight lines were used, for $37 \leq Z \leq 54$ seven were used, for $54 \leq Z \leq 86$ nine were used, and for $Z=90$, 94, 98, and 102 ten were used. With the straight-line approximation, the Schrödinger equation is exactly solvable in terms of Whittaker functions. The approximation leads to the relatively rapid generation of continuum orbitals.

The subshell GOS were calculated using the reduced momentum transfer k' and reduced energy ϵ', where $k'=k/(E_{nl})^{1/2}$ and $\epsilon'=\epsilon/E_{nl}$. The GOS were calculated on a 20×20 grid of (k', ϵ'), and summed up to $l'=12$. The subshell proton ionization cross section is given by[4]

$$\sigma_{nl}=\frac{4\pi a_0^2}{(Me/Mp)E_0}\int_0^{E_0-E_{nl}}\frac{d\epsilon}{(\epsilon+E_{nl})}\times\int_{K^2_{\min}}^{K^2_{\max}}\frac{dK^2}{K^2}\sum_{l'=0}^{\infty}\frac{df_{nl}}{d\epsilon}(\epsilon,K^2,l'), \tag{2}$$

where E_0 is the proton energy in Ry, a_0 is the Bohr radius, M_e and M_p are the electron and proton masses, respectively, and

$$K^2_{\max(\min)}=\frac{M_p}{M_e}[\sqrt{E_0}\pm(\sqrt{E_0}-\epsilon-E_{nl})^{1/2}]^2.$$

The subshell ionization stopping power S_{nl} is obtained by dropping the $(\epsilon+E_{nl})$ denominator in Eq. (2).

The scaling hypothesis is that

$$\sigma_{nl}(E_{nl})^{\alpha_{nl}}=f\left(\frac{M_e}{M_p}\frac{E_0}{E_{nl}}\right)=f(\eta). \tag{3}$$

In classical scaling (E_{nl} large) $\alpha_{nl}=2$. For ionization energies less than the classical scaling threshold, α_{nl} can differ from 2, but there are broad ranges in E_{nl} where an α_{nl} is constant. In each of the broad ranges there is a unique $f(\eta)$, but $f(\eta)$ can differ in the different ranges. α_{nl} is determined by plotting $\sigma_{nl}(\max)E_{nl}^2$ vs E_{nl}, where $\sigma_{nl}(\max)$ is the subshell cross-section maximum. Strictly speaking, this is no hypothesis at all, merely a scaled expression to summarize a large number of calculations. The hypothesis is that Eq. (3), obtained for neutral atoms with the plane-wave Born approximation, is valid for ions. The support for the extension of Eq. (3) to ions is the generally good agreement of Eq. (3) with measurements on inner-shell ionization cross sections over a wide range of projectile energies in neutral atoms. In Sec. II of Ref. 7, several sources of disagreement between the calculations and measurements were discussed. The sources were (1) breakdown of the Born approximation at low energy, (2) choice of central potential in the one-electron model, (3) improper treatment of exchange, (4) breakdown of the one-electron model, (5) neglect of inner-shell excitation followed by autoionization, and (6) experimental inaccuracy. In later calculations,[6] source (5) was eliminated by doing explicit inner-shell excitation calculations. Sources (1) and (3) are of limited significance in these proton calculations as they are limited to $E_0 \geq 0.1(M_p/M_e)E_{nl}$. Source (2) is unimportant as the scaling hypothesis is effectively an averaging over atomic potentials. Source (4) is important when configuration interaction effects are large. However, the comparisons of calculated and measured subshell proton ionization cross sections suggest that the principal source of disagreement is experimental inaccuracy.

The adequacy of the straight-line approximation to the central potential of Herman and Skillman was checked earlier[9] by using four- and five-straight-line approximations to the Ne central potential. In both cases the potential was varied so that the Ne $2p$ eigenvalue agreed with that of Herman and Skillman.[8] The maximum difference between the two sets of GOS was 5%. Manson[10] has presented numerical Herman-Skillman calculations for the $2p$ shell of Al. Because of the choice of continuum electron energies (Manson uses powers of 2 while I use multiples of 5), direct comparison is limited. However, when compared at $\epsilon=0.0$, 1.0, 2.0, and 15/16 Ry, the maximum difference between Manson's and my $2p$ GOS is 20%. This is quite reasonable, as my Al $2p$ eigenvalue (6.38 Ry) differed from the Herman-Skillman[8] (and Manson[10]) $2p$ eigenvalue (5.95 Ry) by 6.7%. To account for the fact that the eigenvalues used in my calculations only approximate those of Herman and Skillman, which themselves only approximate experimental ionization energies, the scaling procedure was developed, allowing one to estimate cross sections using either experimental ionization energies or theoretical eigenvalues.

III. PROTON IONIZATION OF Kr AND Xe

In Fig. 1 the calculated proton ionization cross section of Kr is shown and compared with the measurements of de Heer *et al.*[11] and Gilbody and Lee.[12] The solid line is the ionization cross section ($\sigma_{4p}+\sigma_{4s}+\sigma_{3d}+\sigma_{3p}$) while the dashed line is the electron production cross section ($\sigma_{4p}+\sigma_{4s}+2\sigma_{3d}+3\sigma_{3p}$). In the range of the measurements the two cross sections are identical. The calculated cross section is in excellent agreement with the measurements of

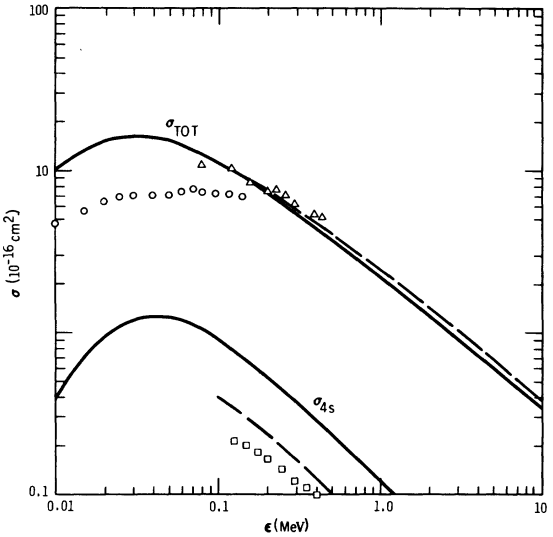

FIG. 1. Proton ionization cross section of Kr. The upper solid curve is $\sum_{nl}\sigma_{nl}$ while the dashed curve is $\sum_{nl}n_{nl}\sigma_{nl}$, where n_{nl} is the ion charge resulting from ionization of the nl subshell. The circles are from Ref. 11 and the triangles from Ref. 12. The lower solid curve is the calculated σ_{4s}, the lower dashed curve is 0.45 σ_{4s} (as discussed in the text), and the squares are the measured 4s cross section of Ref. 13.

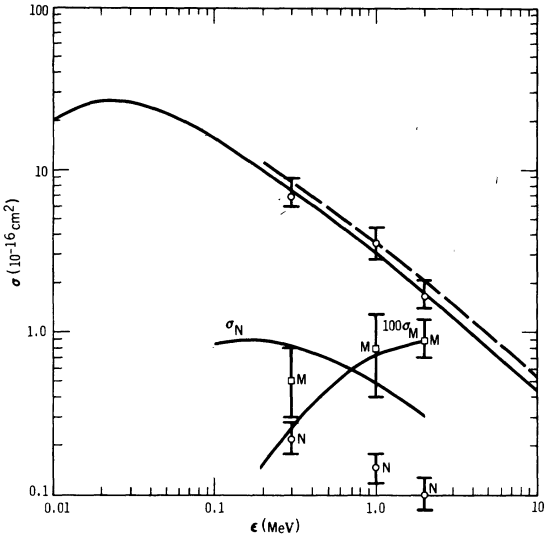

FIG. 2. Proton ionization cross section of Xe. The upper solid curve is $\sum_{nl}\sigma_{nl}$, while the dashed curve is $\sum_{nl}n_{nl}\sigma_{nl}$. The descending lower solid curve is the N-shell cross section while the data points labeled N are measured N-shell cross sections. The ascending lower solid curve is the M-shell cross section times 100, while the data points labeled M are the measured cross sections times 100. All the measurements are from Ref. 15.

Gilbody and Lee,[12] while the measurements of de Heer *et al.*[11] appear to approach the calculations at high energy. Also shown is the calculated σ_{4s}, which is compared with the measurements of Hippler and Schartner,[13] shown as open squares. Hippler and Schartner use the $(4s)^1(4p)^6\ ^2S$-$(4s)^2(4p)^5\ ^2P$ transition to measure the production of 4s vacancies. However, it is known that the $(4s)^1(4p)^6\ ^2S_{1/2}$ level is strongly affected by the configuration interaction, e.g., with $(4s)^2(4p)^4\ ^1D(4d)\ ^2S_{1/2}$. Hansen and Persson[14] calculate that the level designated $(5s)^1(5p)^6\ ^2S_{1/2}$ in Xe contains only 45% $(5s)^1(5p)^6$. Assuming the same percentage composition holds for the level designated $(4s)^1(4p)^6\ ^2S_{1/2}$ in Kr, the calculated cross section for proton ionization of Kr with the ion left in the $(4s)^1(4p)^6\ ^2S_{1/2}$ level is shown as the lower dashed curve in Fig. 1.

In Fig. 2 the calculated proton ionization cross section of Xe and the electron production cross section $(\sigma_{5p}+\sigma_{5s}+2\sigma_{4d}+3\sigma_{4p})$ as well as the measured values of Toburen[15] are shown. Both calculated cross sections are within the error bars of the measurements. Also shown are the calculated N-shell ionization cross section which is a factor of 3–4 larger than the measured values, and the calculated M-shell cross section times one hundred, and measured M-shell values times one hundred. The M-shell calculations are in reasonable agreement with the measurements. Toburen[15] has shown that this M-shell measurements agree and N-shell measurements disagree with cross sections calculated with the binary-encounter approximation (BEA). Toburen[15] attributes the N-shell disagreement to the difficult background subtractions required in using Auger spectra to measure inner-shell ionization cross sections. It will be shown, later, that difficult subtractions in Auger detection are not limited to Xe. In Ref. 7 it was shown that above 1 keV the calculated Xe 4d-electron ionization cross section agreed to 20% with the measured values. However, the experimental cross section was taken to be the cross section for production of Xe^{+2} as measured by El Sherbini *et al.*[16] Since the 4d-ionization cross section should be comparable for 1-keV electrons and 2-MeV protons, and the Xe N-shell cross section is dominated by 4d ionization, it appears that the discrepancy between calculated and measured proton ionization cross sections arises from the use of the Auger spectrum as an ionization detector.

Xe is the highest-Z element for which calculations were done on the 2s- and 2p-subshell proton ionization cross section. The calculations are shown in Fig. 3, along with rescaled measurements on U by Barros Leite *et al.*[17] That is, if σ(U) is the uranium cross section at proton energy E(U), the rescaled data are $\sigma(\mathrm{Xe})=\alpha^2\sigma(\mathrm{U})$ and $E(\mathrm{Xe})=E(\mathrm{U})/\alpha$, where $\alpha=E_I(\mathrm{U})/E_I(\mathrm{Xe})$ and E_I is the subshell ionization energy. The rescaled data on

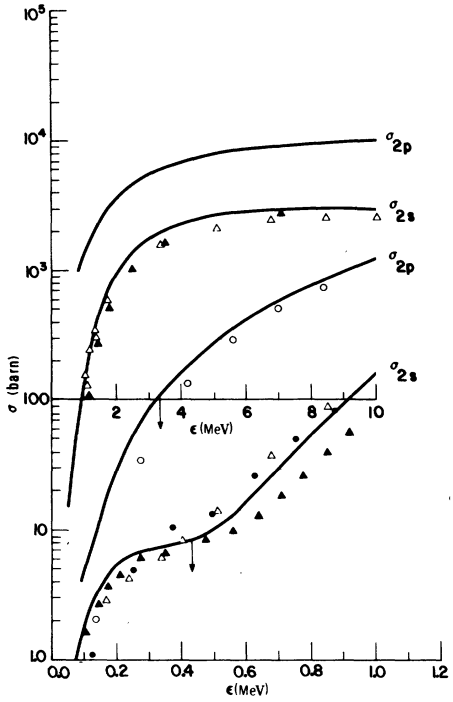

FIG. 3. The plateau region in the 2*s* proton ionization cross section. The lower (upper) two curves refer to the lower- (upper-) energy axis. The calculations are for Xe while the data are for other elements, rescaled to Xe as discussed in the text. The solid circles are the rescaled U 2*s* ionization cross-section measurements of Ref. 17, while the open and closed triangles are rescaled Ar and Kr calculations. The open circles are the rescaled 2*p* ionization cross-section measurements of Ref. 17.

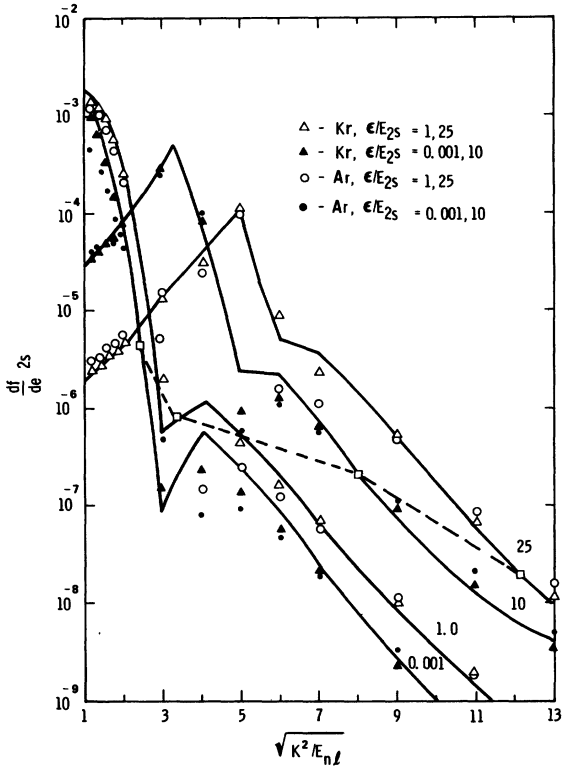

FIG. 4. Xe (solid line) 2*s* GOS versus scaled momentum transfers $(K^2/E_{2s})^{1/2}$ with scaled energy (ϵ/E_{2s}) as parameter. The triangles (circles) are Kr(Ar) GOS normalized to the Xe data at $(K^2/E_{2s})^{1/2}=5$ and $\epsilon/E_{2s}=25$.

U is compared with the Xe calculations to show the persistence (and scalability) of the plateau region in the 2*s* cross section for high-Z elements. Also shown are the *calculated* 2*s* cross sections for Ar and Kr, rescaled to Xe. The calculations exhibit a plateau region comparable to that measured in U, while the Kr calculation shows the most pronounced plateau. The Kr calculation shows scalability is only approximate (factor of 2) in the plateau region. However, the cross section is small in this region and does not contribute significantly to the stopping power.

Kim *et al.*[18] have pointed out that in excitation, a zero in the GOS can lead to a minimum in the cross section. Manson and Msezane[19] extended the analysis to ionization. They pointed out that because all angular momentum components are allowed in the continuum and because one integrates over secondary electron energy, the GOS would not be expected to have a zero but could have a minimum, and the minimum would lead to a plateau region in the cross section. Figure 3 indicates that for the 2*s* subshell the plateau occurs at roughly the same scaled energy from Ar to U. In Fig. 4 the GOS for the 2*s* subshell in Xe is plotted as solid lines as a function of scaled momentum transfer $[(K^2/E_{2s})^{1/2}]$ with scaled continuum electron energy as parameter, for $\epsilon/E_{2s}=0.001$, 1, 10, and 25. A minimum, most pronounced at small ϵ/E_{2s}, is clearly seen (no such minimum appears in the 2*p* GOS). In scaled units the lower limit in the momentum-transfer integral [Eq. (2)] is

$$(K^2_{\min}/E_{2s})=(1+\epsilon/E_{2s})/4\eta_{2s}\,.$$

For $\eta_{2s}=0.043$ corresponding to 400-keV protons in Xe (in the plateau region), the dashed line in Fig. 4 connects the lower limits in the momentum-transfer integrals. In computing the cross section, one integrates from infinite to minimum momentum transfer. For $\epsilon=0.001$, 10, and 25 the GOS is rapidly increasing but at $\epsilon=1$, the GOS is decreasing. Coupled with the $1/E_0$ term in the cross-section expression, the decrease in GOS near $\epsilon=1$ leads to the plateau region. This is essentially the argument of Manson and Msezane.[19]

Why the plateau region remains fixed in scaled variables is an additional question. For this to oc-

cur, the GOS must scale. In Fig. 4 the GOS for Ar and Kr is plotted in scaled variables. The Ar and Kr GOS are normalized to Xe at the $\epsilon/E_{2s}=25$ peak, i.e., the Kr(Ar) GOS is reduced by a factor 0.293 (0.0453). The scaled Kr GOS (open triangles at $\epsilon/E_{2s}=1$ and 25, solid triangles at $\epsilon/E_{2s}=0.001$ and 10) and Ar GOS (open circles at $\epsilon/E_{2s}=1$ and 25, solid circles at $\epsilon/E_{2s}=0.001$ and 10) are in reasonable agreement (on a semilog plot) with the scaled Xe GOS at small and large $(K^2/E_{2s})^{1/2}$ but there is considerable variation at the minimum. This accounts for the above-mentioned factor-of-2 limitation on the scaled cross section in the plateau region. It should be noted that the minimum in the 2s GOS occurs beyond the Bethe ridge ($\epsilon=K^2$), where the cross sections are extremely small. Finally, the factors used to scale the Ar and Kr GOS to Xe, 0.0453 and 0.293, respectively, are reasonably close to the ratios of ionization energies, 0.064 and 0.350, respectively, suggesting that the subshell GOS may be scaled as

$$\frac{df_{nl}}{d\epsilon}(\epsilon,k^2)=\frac{1}{E_{nl}}\beta_{nl}H_{nl}\left(\frac{\epsilon}{E_{nl}},\frac{k^2}{E_{nl}}\right),$$

where H is a scaling function, and $\beta_{nl}=1$ for E_{nl} large.

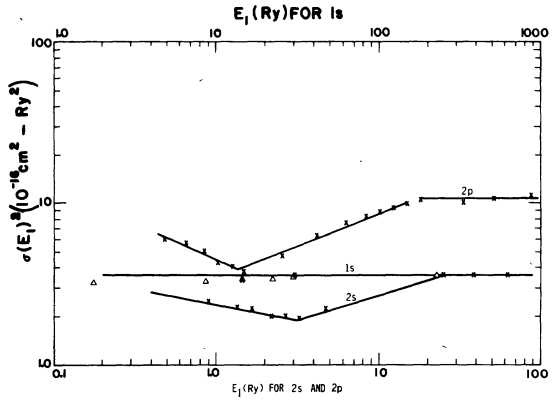

FIG. 5. Calculated $(\sigma_{nl})_{\max}E_{nl}^2$ for the 1s, 2s, and 2p subshells.

IV. THE SCALED 1s, 2s, AND 2p PROTON IONIZATION CROSS SECTIONS

In Fig. 5, $(\sigma_{nl})_{\max}E_{nl}^2$ is plotted versus E_{nl} for the 1s, 2s, and 2p subshells. For the 1s subshell there is a 10% increase in $(\sigma_{1s})_{\max}E_{1s}^2$ in going from the lowest E_{1s}(He) to the highest E_{1s}(Ar). For simplicity the scaled 1s cross section is represented by one scaling function obtained from the Ar 1s

TABLE I. Parameters for the scaled 1s, 2s, and 2p proton ionization cross sections; $\sigma_{nl}(E_p)(E_{nl})^{\alpha_{nl}}=f_i(M_e E_p/M_p E_{nl})$ with f in units of 10^{-16} cm^2 Ry$^{\alpha}$. The subscripts a–c refer to the following values of α_{nl} and E_{nl}~.

1s $\alpha=2.00$		2s a: $0.4\leq E_I\leq 3.1$, $\alpha=2.19$ b: $3.1\leq E_I\leq 24.5$, $\alpha=1.70$ c: $E_I\geq 24.5$, $\alpha=2.00$				2p a: $0.5\leq E_I\leq 1.4$, $\alpha=2.44$ b: $1.4\leq E_I\leq 28.0$, $\alpha=1.59$ c: $E_I\geq 28.0$, $\alpha=2.00$			
η	f	η	f_a	f_b	f_c	η	f_a	f_b	f_c
0.03	0.017								
0.05	0.072								
0.07	0.165								
0.10	0.36	0.10	0.50	0.36	0.22	0.10	0.65	0.50	1.15
0.15	0.72	0.15	0.80	0.52	0.63	0.15	1.10	0.80	2.20
0.20	1.06	0.20	1.08	0.67	1.10	0.20	1.55	1.10	3.25
0.30	1.70	0.30	1.50	0.90	2.00	0.30	2.25	1.60	5.10
0.50	2.70	0.50	2.00	1.17	3.10	0.50	3.20	2.25	7.50
0.70	3.25	0.70	2.23	1.31	3.50	0.70	3.75	2.70	9.20
1.00	3.60	1.00	2.40	1.38	3.60	1.00	4.20	3.00	10.3
1.50	3.60	1.50	2.30	1.32	3.35	1.50	4.40	3.25	10.8
2.00	3.40	2.00	2.10	1.24	3.00	2.00	4.40	3.25	10.6
3.0	2.95	3.0	1.75	1.05	2.40	3.0	4.10	3.05	9.5
5.0	2.35	5.0	1.30	0.79	1.70	5.0	3.50	2.60	7.5
7.0	1.90	7.0	1.05	0.62	1.35	7.0	2.95	2.20	6.2
10.0	1.50	10.0	0.80	0.47	1.02	10.0	2.45	1.80	4.9
15.0	1.05	15.0	0.57	0.35	0.74	15.0	1.86	1.38	3.7
20.0	0.82	20.0	0.45	0.275	0.58	20.0	1.50	1.10	3.0
30.0	0.57	30.0	0.32	0.196	0.41	30.0	1.10	0.80	2.25
50.0	0.35	50.0	0.21	0.127	0.265	50.0	0.73	0.54	1.50
70.0	0.25	70.0	0.155	0.095	0.195	70.0	0.56	0.40	1.15
100.0	0.18	100.0	0.114	0.070	0.145	100.0	0.42	0.30	0.85

cross section. For the $2s$ and $2p$ cross sections three scaling functions are used. These are given in Table I. Asymptotically,

$$(\sigma_{1s})_{max}(E_{1s})^2 = (\sigma_{2s})_{max}(E_{2s})^2 = (\sigma_{2p})_{max}(E_{2p})^2/3 .$$

In Fig. 6 the scaled $1s$ cross section is shown and compared with experimental measurements. Several of the older experiments obtain ionization cross sections from x-ray emission cross sections using K-shell fluorescence yields lower than the best estimates in Bambynek *et al.*[20] These experimental cross sections have been corrected to the fluorescence yields of Bambynek *et al.*[20] The measurements in Fig. 6 are not exhaustive, but cover an extensive portion of the periodic table. All ionization energies used in scaling the measurements are from the electron spectroscopy for chemical analysis (ESCA) tabulation.[21]

The He *measurements* of de Heer *et al.*,[11] open squares, are somewhat lower than the scaled cross section and peak at a somewhat high value of η, but are in reasonable agreement asymptotically. However, the He *calculations* are in reasonable agreement with the scaled cross section from the Ar calculations; i.e., there is no shape variation with E_{1s} in the calculations. The Al measurements of Khan *et al.*[22] are in excellent agreement with the scaled $1s$ cross section when ω_K is changed from 0.029[22] to 0.038.[20] The measurements of Bissinger *et al.*[23] on Ca (open circles) are in excellent agreement, and those on Ti and Ni (slashed circles) are in good agreement with the scaled cross section, when the ω_K values are changed from 0.120, 0.170, and 0.359,[23] respectively, to 0.163, 0.219, and 0.414.[20] The Ag measurements of Bissinger *et al.*[24] (solid circles) are in excellent agreement with the scaled cross section with $\omega_K = 0.821$.[24] The "most reliable" experimental value of ω_K is 0.834, while three independently calculated values are $\omega_K = 0.842$, 0.844, and 0.861.[20] The choice of ω_K could lower the experimental cross section by 5%.

The points shown as open triangles are the corrected measurements of Jarvis *et al.*[25] for 160-MeV protons on a variety of elements from Fe to U. The corrected measurements use the ω_K values of Ref. 20 rather than the ω_K values of Jarvis *et al.*[25] In addition the measurements were corrected for relativistic projectile effects. Arthurs and Moiseiwitsch[26] have shown for electron ionization of the $1s$ shell that a relativistic treatment introduces a factor γ^2 multiplying the nonrelativistic cross section. There are additional relativistic effects but these involve integrals over the GOS. The data of Jarvis *et al.*[25] are compared with the scaled cross section by reducing the measured cross section by γ^{-2} where $\gamma^2 = 1.37$. Jarvis *et al.*[25] compare their measurements with nonrelativistic

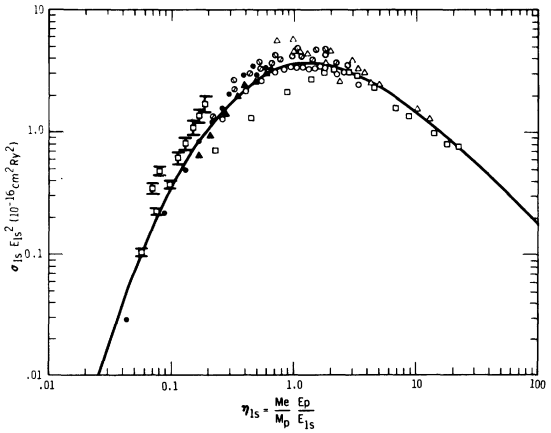

FIG. 6. The scaled $1s$ proton ionization cross section and scaled measurements. The open squares are He measurements of Ref. 11, the solid triangles are Al measurements of Ref. 22, the open and slashed circles are Ca, Ti, and Ni measurements from Ref. 23, the solid circles are the Ag measurements of Ref. 24, the open triangles are corrected measurements from Ref. 25 on a variety of elements from Fe to U at 160 MeV, and the solid squares with error bars are Kr and Xe measurements from Ref. 28.

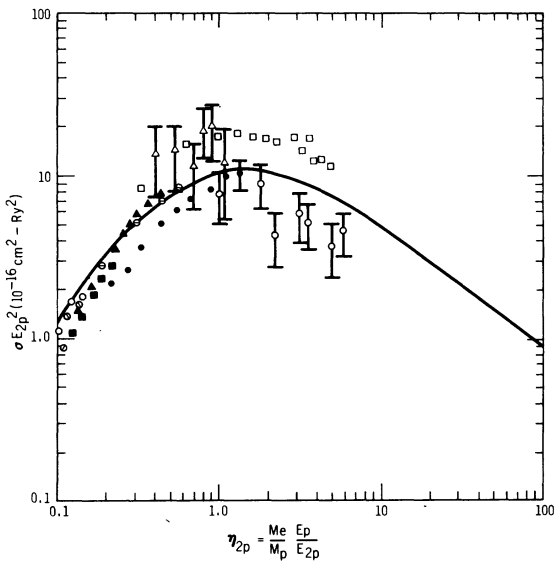

FIG. 7. The scaled $2p$ proton ionization cross section and scaled measurements. The solid circles and open circles with error bars are Ar measurements from Refs. 30 and 32, respectively, the open triangles with error bars are Zn measurements from Ref. 31, the open squares are Ag measurements from Ref. 24, the solid triangles and squares are Sn and Dy measurements of Ref. 40, the open and diagonally slashed circles are measurements on Au, Pb, and U from Ref. 17, and the horizontally slashed open circles are U measurements of Ref. 29.

TABLE II. Comparison of the numerical Herman and Skillman calculations of σ_{2s} and σ_{2p} (Ref. 42) with our direct (mod) and scaled cross sections.

Proton energy (MeV)	$\sigma(10^{-19}$ cm$^2)$ $\sigma_{2s(\text{num})}$	$\sigma_{2s(\text{mod})}$	$\sigma_{2s(\text{scaled})}$	$\sigma_{2p(\text{num})}$	$\sigma_{2p(\text{mod})}$	$\sigma_{2p(\text{scaled})}$
0.12	2.47	2.16	3.45	13.2	12.9	13.9
0.3	6.26	5.77	5.92	26.3	26.1	25.5
0.7	7.28	6.70	6.80	31.6	31.3	31.9
1.5	5.54		5.57	26.9		29.4
3.0	3.58	3.24	3.80	19.1	18.6	22.3
8.0	1.68	1.54	1.80	9.83	9.62	12.2
20.0	0.79		0.85	4.89		5.83

calculations by dividing their measurements by 1.26, based on velocity arguments, i.e., $(v_{NR})^2 = (2)(160/938)c^2$ and $(v_R)^2 = (1 - 1/\gamma^2)c^2$, and $(v_{NR}/v_R) = 1.26$. With the exception of the cross sections for Pb and U, all the measurements of Jarvis *et al.*[25] at 160 MeV, with the Arthurs and Moiseiwitsch[26] relativistic factor, are in good agreement with the scaled cross section. The disagreement for Pb and U is not surprising as the only correction made for relativistic effects on the 1*s* orbital is the use of the measured ionization energy.

Akselsson and Johansson[27] have remeasured the Ag proton ionization cross section. Their results are slightly lower than those of Bissinger *et al.*[24] (the solid circles in Fig. 6). The measurements of Winters *et al.*[28] in Kr and Xe, shown as solid squares with error bars in Fig. 6, are considerably higher than the scaled measurements, i.e., a factor of 1.7 at 5 MeV in Kr ($\eta = 0.19$) and 2.0 at 5 MeV in Xe ($\eta = 0.08$). From 1.5 to 5.0 MeV the Ar measurements of Winters *et al.*[28] are within ten percent of the scaled cross section. The Kr and Xe measurements of Winters *et al.*,[28] if correct, would cast doubt on the scaling hypothesis. However, the Kr and Xe measurements cannot be reconciled with the two independent Ag measurements (e.g., if relativistic effects on the 1*s* orbital are more important for small η than for large η); one would expect $\sigma(\text{Xe}) > \sigma(\text{Ag}) > \sigma(\text{Kr})$ at fixed η suggesting that the Kr and Xe measurements are in error.

In Fig. 7 the scaled 2*p* cross section in the classical region is shown and compared with scaled experimental measurements. In addition to corrections to fluorescence yields used in older measurements, two other corrections were made. When a total *L*-shell cross section is measured, a theoretical 2*s* cross section, found from Table I, is subtracted. This is a less than 25% correction. When both L_2 and L_3 cross sections are measured, the 2*p* cross section is taken to be the L_3 cross section multiplied by 1.5.

The open circles and circles with diagonal slashes are the scaled L_3 measurements of Barros Leite *et al.*[17] on Au, Pb, and U, and are in good agreement with the scaled cross section. The open circles with horizontal slashes are the scaled U measurements of Li *et al.*,[29] in excellent agreement with the scaled cross sections. Both sets of measurements are for the L_3 cross section and use the fluorescence yields of Ref. 20. The solid circles are the Ar measurements of Stolterfoht *et al.*,[30] with the theoretical 2*s* cross section subtracted. As with the He measurements in Fig. 5, the Ar measurements are lower than the scaled cross section at low η. Since the scaled cross section is based in the Ar 2*p* calculations, this disagreement is clearly an inaccuracy in the Born approximation. The open triangles with error bars and circles with error bars are the measurements on Zn of Kojima *et al.*[31] and the Ar measurements of Maeda *et al.*,[32] both using the 2*p* Auger electron spectrum to measure the ionization cross section. The Zn measurements,[31] even with large error bars, are higher than the scaled cross section, while the Ar measurements[32] are lower than the scaled cross section. With error bars included, the highest energy point of Stolterfoht *et al.*[30] (at $\eta = 1.35$), is consistent with the lowest energy

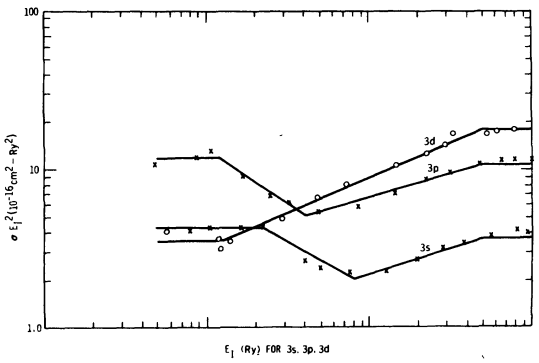

FIG. 8. Calculated $(\sigma_{nl})_{\max} E_{nl}^2$ for the 3*s*, 3*p*, and 3*d* subshells.

TABLE III. Parameters for the scaled $3s$, $3p$, and $3d$ proton ionization cross sections; $\sigma_{nl}(E_p)(E_{nl})^{\alpha_{nl}} = f_i(M_e E_p/M_p E_{nl})$, with f in units of 10^{-16} cm^2 Ry$^{\alpha}$. The subscripts a–d refer to the following values of α_{nl} and E_{nl}.

	$3s$				$3p$				$3d$		
	a: $0.5 \leq E_I \leq 2.2$, $\alpha = 2.00$				a: $0.5 \leq E_I \leq 1.2$, $\alpha = 2.00$				a: $0.5 \leq E_I \leq 1.3$, $\alpha = 2.00$		
	b: $2.2 \leq E_I \leq 8.0$, $\alpha = 2.56$				b: $1.2 \leq E_I \leq 4.2$, $\alpha = 2.67$				b: $1.3 \leq E_I \leq 50$, $\alpha = 1.555$		
	c: $8.0 \leq E_I \leq 50.0$, $\alpha = 1.67$				c: $4.2 \leq E_I \leq 48$, $\alpha = 1.71$				c: $50 \leq E_I$, $\alpha = 2.00$		
	d: $50.0 \leq E_I$, $\alpha = 2.00$				d: $48 \leq E_I$, $\alpha = 2.00$						
η	f_a	f_b	f_c	f_d	f_a	f_b	f_c	f_d	f_a	f_b	f_c
0.10		0.72	0.065	0.17		2.30	0.38	0.90		0.69	2.15
0.15		1.90	0.175	0.58		4.45	0.72	2.05		1.00	3.70
0.20	2.05	3.10	0.300	1.05		6.30	1.05	3.40		1.30	5.20
0.30	3.00	4.70	0.53	2.00		9.10	1.65	5.60	2.45	1.72	7.70
0.50	4.10	6.25	0.83	3.10	9.70	12.0	2.50	8.60	3.08	2.30	11.50
0.70	4.50	6.50	0.97	3.60	11.3	13.2	3.00	10.30	3.37	2.67	14.0
1.00	4.20	6.25	1.01	3.60	11.8	13.2	3.40	11.0	3.60	2.96	16.5
1.50	3.60	5.50	0.94	3.30	11.6	12.5	3.40	10.5	3.65	3.20	18.0
2.00	3.00	4.70	0.85	2.80	10.9	11.5	3.20	9.50	3.60	3.20	17.5
3.0	2.20	3.65	0.70	2.20	9.00	9.60	2.80	7.90	3.45	3.10	16.0
5.0	1.43	2.60	0.49	1.60	6.90	7.30	2.10	5.90	3.05	2.80	13.0
7.0	1.08	2.00	0.38	1.25	5.60	5.70	1.68	4.65	2.77	2.50	
10.0	0.78	1.50	0.29	1.00	4.40	4.40	1.32	3.55	2.35	2.03	
15.0	0.53	1.08	0.21		3.25	3.25	0.98		1.90	1.60	
20.0	0.40	0.83	0.165		2.55	2.55	0.80		1.60	1.32	
30.0	0.28	0.58	0.120		1.85	1.85	0.58		1.25	1.00	
50.0	0.17	0.36	0.079		1.20	1.20	0.39		0.87	0.69	
70.0	0.12	0.27	0.059		0.87	0.87	0.29		0.67	0.54	
100.0	0.085	0.195	0.044		0.63	0.63	0.22		0.52	0.41	

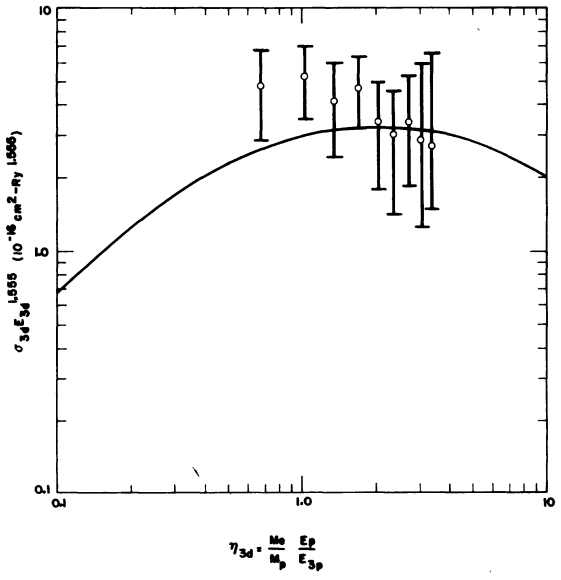

FIG. 9. The nonclassical scaled $3d$ cross section ($1.3 \leq E_{3d} \leq 50$ Ry) and the scaled Cd measurements of Ref. 31.

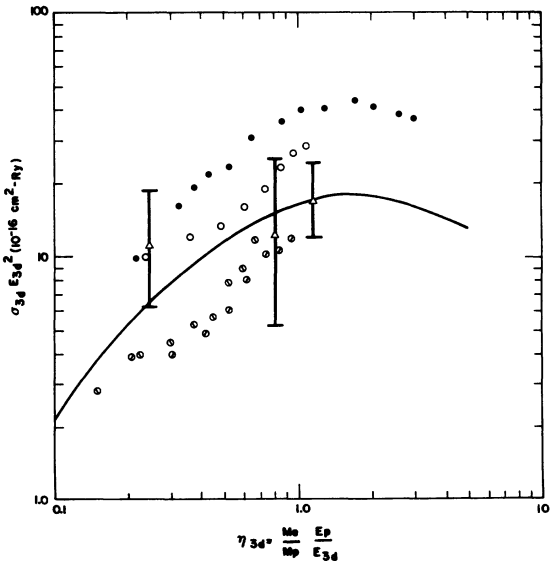

FIG. 10. The classical scaled $3d$ proton ionization cross section and scaled measurements. The triangles with error bars are the Xe measurements of Ref. 15, the open and slashed circles are measurements on Au, Bi, and U from Ref. 44, and the solid circles are Pb measurements of Ref. 43.

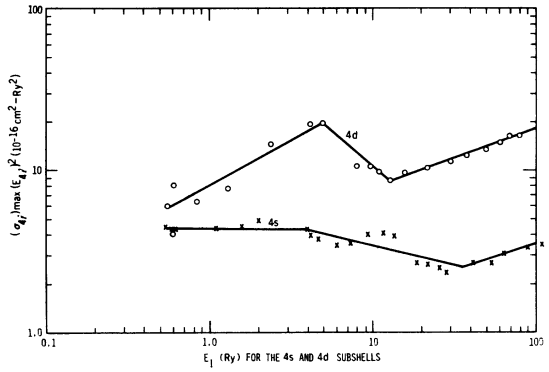

FIG. 11. Calculated $(\sigma_{nl})_{\max} E_{nl}^2$ for the $4s$ and $4d$ subshells.

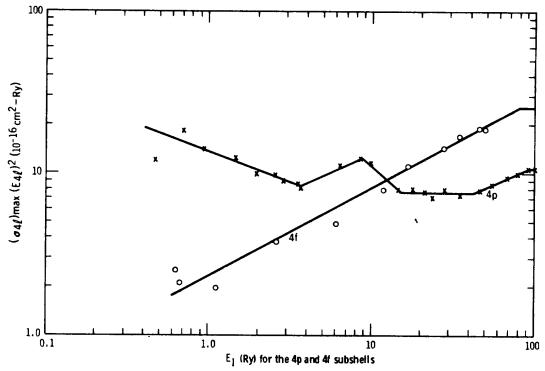

FIG. 12. Calculated $(\sigma_{nl})_{\max} E_{nl}^2$ for the $4p$ and $4f$ subshells.

point (at $\eta = 1.75$) of Maeda *et al.*[32] In Ref. 5 it was shown that the $2p$ electron ionization cross-section measurements on Ar of Langeberg *et al.*[33] were in excellent agreement with the scaled $2p$-electron ionization cross section at large η. Langenberg *et al.*[33] used x-ray detection to measure the cross section. This suggests that the discrepancy between the scaled $2p$ proton ionization cross section and the measurements in Refs. 31 and 32 is an artifact of the Auger detection technique.

The measurements of Bissinger *et al.*[24] on Ag (open squares in Fig. 7) are significantly higher than the scaled cross section, even after a correction for mean fluoresence yield. Bissinger *et al.*[24] use $\omega_{\bar{L}} = 0.047$, measured by Bertrand *et al.*[34] Bailey and Swedlund[35] measure $\omega_{\bar{L}} = 0.066$. Chen *et al.*[36] calculate $\omega_{L_3} \sim \omega_L = 0.046$, I[37] calculate $\omega_{\bar{L}} = 0.061$, while Walters and Bhalla[38] calculate $\omega_{\bar{L}} = 0.063$. I have used $\omega_{\bar{L}} = 0.061$ rather than the value $\omega_{\bar{L}} = 0.047$ used by Bissinger *et al.*,[24] and, in addition,

TABLE IV. Parameters for the scaled $4s$ and $4p$ proton ionization cross sections; $\sigma_{nl}(E_p)(E_{nl})^{\alpha_{nl}} = f_i(M_e E_p / M_p E_{nl})$ with f in units of $10^{-16}\,\mathrm{cm}^2\,\mathrm{Ry}^{\alpha}$. The subscripts a–f refer to the following values of α_{nl} and E_{nl}.

	$4s$				$4p$					
	a: $0.5 \leq E_I \leq 4.0$, $\alpha = 2.00$				a: $0.4 \leq E_I \leq 3.6$, $\alpha = 2.37$					
	b: $4.0 \leq E_I \leq 35$, $\alpha = 2.25$				b: $3.6 \leq E_I \leq 8.5$, $\alpha = 1.55$					
	c: $35 \leq E_I \leq 100$, $\alpha = 1.67$				c: $8.5 \leq E_I \leq 15$, $\alpha = 2.80$					
	d: $E_I \geq 100$, $\alpha = 2.00$				d: $15 \leq E_I \leq 43$, $\alpha = 2.00$					
					e: $43 \leq E_I \leq 90$, $\alpha = 1.56$					
					f: $E_I > 90$, $\alpha = 2.00$					
η	f_a	f_b	f_c	f_d	f_a	f_b	f_c	f_d	f_e	f_f
0.10	0.28	0.50	0.063	0.19	1.32	0.85	8.5	1.07	0.105	0.69
0.15	0.78	1.40	0.164	0.57	2.80	1.70	18.0	2.20	0.23	1.75
0.20	1.37	2.30	0.265	1.02	4.20	2.35	27.0	3.20	0.39	2.90
0.30	2.42	3.70	0.435	1.87	6.70	3.45	42.0	4.80	0.67	5.40
0.50	3.85	5.40	0.660	3.00	10.1	4.40	60.0	6.60	1.10	8.40
0.70	4.40	6.00	0.760	3.45	12.2	4.60	67.0	7.40	1.32	9.80
1.00	4.40	6.00	0.790	3.66	13.2	4.45	68.0	7.60	1.42	10.5
1.50	3.72	5.20	0.730	3.26	12.7	3.95	63.0	7.10	1.36	9.90
2.00	3.17	4.60	0.665	2.85	11.8	3.45	57.0	6.40	1.22	8.80
3.0	2.35	3.60	0.540	2.35	10.0	2.75	45.5	5.20	1.00	7.20
5.0	1.50	2.50	0.395	1.75	7.50	1.90	32.5	3.70	0.73	5.00
7.0	1.10	1.95	0.310		6.00	1.47	25.5	2.85	0.58	
10.0	0.78	1.45	0.235		4.60	1.12	19.5	2.20		
15.0	0.53	1.00			3.35	0.79	14.0	1.55		
20.0	0.40	0.76			2.65	0.62	11.1	1.23		
30.0	0.27	0.52			1.85	0.43	7.8			
50.0	0.165	0.31			1.20	0.275				
70.0	0.118	0.22			0.90	0.205				
100.0	0.081	0.15			0.66	0.150				

TABLE V. Parameters for the scaled $4d$ and $4f$ proton ionization cross sections; $\sigma_{nl}(E_p)(E_{nl})^{\alpha_{nl}} = f_i(M_e E_p / M_p E_{nl})$ with f in units of 10^{-16} cm^2 Ry$^{\alpha}$. The subscripts a–d refer to the following values of α_{nl} and E_{nl}.

	$4d$				$4f$			
	a: $0.6 \leq E_I \leq 5.0$, $\alpha = 1.46$				a: $0.6 \leq E_I \leq 1.7$, $\alpha = 1.46$			
	b: $5.0 \leq E_I \leq 13.$, $\alpha = 2.88$				b: $1.7 \leq E_I \leq 14$, $\alpha = 1.46$			
	c: $13 \leq E_I \leq 100$, $\alpha = 1.62$				c: $14 \leq E_I \leq 80$, $\alpha = 1.46$			
	d: $E_I \geq 100$, $\alpha = 2.00$				d: $E_I \geq 80$, $\alpha = 2.00$			
η	f_a	f_b	f_c	f_d	f_a	f_b	f_c	f_d
0.10	1.37	14.8	0.48	2.00		0.65	0.38	3.6
0.15	2.25	23.4	0.82	3.80		0.93	0.57	5.5
0.20	3.00	31.0	1.13	5.60		1.17	0.75	7.2
0.30	4.30	44.0	1.65	8.70		1.51	1.02	10.0
0.50	6.10	62.0	2.40	13.2	2.20	1.90	1.43	14.5
0.70	7.20	72.0	2.85	16.1	2.22	2.12	1.72	18.0
1.00	7.90	79.0	3.17	18.2	2.18	2.28	2.00	21.4
1.50	8.30	80.0	3.20	18.6	2.05	2.30	2.25	24.5
2.00	8.20	77.0	3.00	17.6	1.90	2.30	2.38	26.0
3.0	7.60	68.0	2.70	15.3	1.72	2.25	2.40	25.0
5.0	6.50	55.0	2.10	11.8	1.44	2.03	2.05	21.8
7.0	5.60	45.0	1.68	9.4	1.26	1.83	1.80	18.8
10.0	4.60	36.0	1.30		1.08	1.61	1.55	15.5
15.0	3.60	26.5	0.96		0.89	1.36	1.23	
20.0	2.95	21.5	0.78		0.78	1.17		
30.0	2.20	15.8	0.56		0.63	0.90		
50.0	1.48	10.5	0.37		0.45	0.64		
70.0	1.14	8.1			0.36	0.50		
100.0	0.85	5.9			0.28	0.38		
150.0					0.21	0.27		
200.0					0.17			
300.0					0.13			
400.0					0.10			

have subtracted a theoretical $2s$ cross section in plotting the Ag measurements in Fig. 7. Even with the corrected $\omega_{\bar{L}}$, the measurements of Bissinger *et al.*[24] are a factor of 1.7 larger than the scaled $2p$ cross section. Chaturvedi *et al.*[39] measure an Ag L-shell ionization cross section slightly larger than that of Bissinger *et al.* In addition Chaturvedi *et al.*[39] present measurements on L-shell proton ionization in Sn. They measure an L-shell x-ray production cross section of 1270 b at 3 MeV. But both Khan *et al.*[40] and Ishi *et al.*[41] measure a cross section of 860 b at 3 MeV. Thus the measurements of Chaturvedi *et al.*[39] are a factor of 1.5 larger than the measurements of Refs. 40 and 41 for Sn

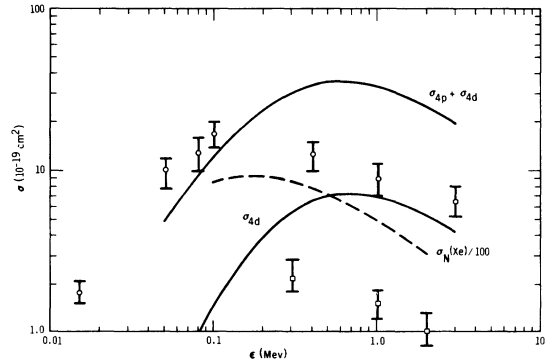

FIG. 13. The solid curves are the calculated $4p$ and $4p+4d$ proton ionization cross sections of W. The open circles with error bars are the measurements of Ref. 47. The dashed curve and open squares with error bars are the Xe N-shell calculated and measured cross sections reduced by a factor of 100.

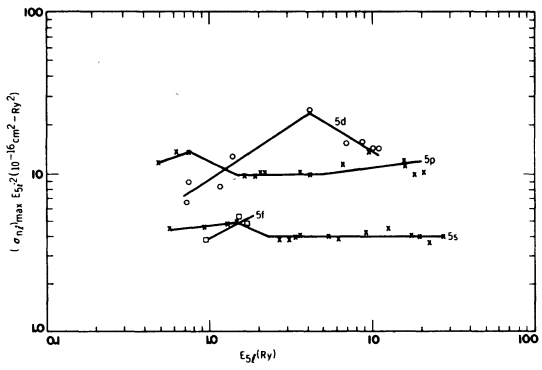

FIG. 14. Calculated $(\sigma_{nl})_{\max} E_{nl}^2$ for the $5s$, $5p$, $5d$, and $5f$ subshells.

($Z=50$), but in agreement with the Ag measurements of Bissinger *et al.*[24] The solid triangles and squares are the measurements of Khan *et al.*[40] for Sn and Dy, respectively, where I have used $\omega_L(\mathrm{Sn})=0.074$ and $\omega_L(\mathrm{Dy})=0.180$.[20] They are in good agreement with the scaled $2p$ cross section. There is a clear discrepancy between the measurements of Refs. 24 and 39 and Refs. 40 and 41, and the calculations support the latter measurements.

Choi[42] has done numerical Herman-Skillman calculations on the $2s$ and $2p$ subshells of argon. He presents $F(K^2)=(K^2/\Delta E)df(K^2)/d\epsilon$ in a graphical form. Because $df(K^2)/d\epsilon=C_1+C_2K^2$ for small K^2, Choi's $F(K^2)$ is presented in log-log form, making a direct comparison of calculated $f(K^2)$ difficult. However, Choi[42] presents $2s$ and $2p$ proton ionization cross sections and in Table II, I intercompare Choi's $2s$ and $2p$ cross sections with my direct calculations (mod) and my scaled cross sections. Except at the lowest energy 0.12 MeV where $\eta_{2s}=0.21$, both the model cross-section calculation and the scaled cross-section calculation agree with Choi's results to better than 10%. For the $2p$ cross section, the model calculation agrees with Choi's results to better than 3%. The scaled $2p$ cross section is in excellent agreement (3%) below 1 MeV, but differs above 1 MeV by as much as 25%. For large η there can be a variation of as much as 50% in the scaled cross section obtained from individual elements at the beginning and end of a range of E_I with constant α, even when the variation in peak cross section is much smaller. This accounts for the 25% error in the argon $2p$ cross section calculated with f_b of Table I.

V. THE SCALED $3s$, $3p$, AND $3d$ PROTON IONIZATION CROSS SECTIONS

In Fig. 8, $(\sigma_{nl})_{\max}E_{nl}^2$ is shown versus E_{nl} for the $3s$, $3p$ (crosses), and $3d$ (circles) subshells. The parameters in the scaled cross sections are listed in Table III. To compare the limited data with the scaled cross sections, a procedure, similar to that used for the L-shell, was adopted. As the measurements are for total M-shell ionization, I first subtracted a $3p$ cross section (from Table III) to obtain a measured $3d$ cross section. The $3p$ contribution can be as much as 40%. In Fig. 9 the non-

TABLE VI. Parameters for the scaled $5s$, $5p$, $5d$, and $5f$ proton ionization cross sections: $\sigma_{nl}(E_p)(E_{nl})^{\alpha_{nl}}=f_i(M_eE^p/M_pE_{nl})$ with f in units of 10^{-16} cm^2 Ry$^\alpha$. The subscripts a–d refer to the following values of α_{nl} and E_{nl}.

$5s$			$5p$			$5d$			$5f$
a: $0.5\le E_I\le 1.5$,	$\alpha=1.88$		a: $0.4\le E_I\le 0.65$,	$\alpha=1.65$		a: $0.7\le E_I\le 4.0$,	$\alpha=1.33$		a: $1.0\le E_I\le 1.7$, $\alpha=1.50$
b: $1.5\le E_I\le 2.3$,	$\alpha=2.46$		b: $0.65\le E_I\le 1.5$,	$\alpha=2.50$		b: $4.0\le E_I\le 11.0$,	$\alpha=2.60$		
c: $2.3<E_I\le 27.0$,	$\alpha=2.00$		c: $1.5\le E_I\le 5.0$,	$\alpha=2.00$					
			d: $5.0\le E_I\le 20.0$,	$\alpha=1.88$					

η	f_a	f_b	f_c	f_a	f_b	f_c	f_d	f_a	f_b	f_a
0.10			0.155			0.50	0.62	1.32	6.5	
0.15			0.520			1.33	1.55	2.13	11.4	
0.20			1.00			2.22	2.70	2.90	16.2	
0.30	2.86	3.40	2.05			3.85	4.80	4.20	24.5	2.20
0.50	4.25	5.20	3.45	11.8	9.4	6.40	7.50	6.00	37.5	2.90
0.70	4.70	5.90	4.00	13.5	10.7	8.10	8.50	7.25	46.0	3.40
1.00	4.70	5.85	3.85	15.0	11.6	9.40	8.30	8.30	54.0	3.70
1.50	4.05	5.10	3.20	15.0	11.7	9.70	7.40	9.20	56.0	3.90
2.00	3.40	4.30	2.72	14.0	11.0	9.00	6.20	9.20	54.0	4.00
3.00	2.60	3.15	2.05	12.2	9.3	7.50	4.65	8.80	47.5	4.00
5.0	1.73	2.05	1.36	9.20	7.2	5.40	3.10	7.60	38.0	3.75
7.0	1.30	1.55	1.03	7.40	5.7	4.20	2.35	6.50	30.0	3.45
10.0	0.93	1.12	0.76	5.80	4.4	3.25	1.75	5.20	24.4	3.05
15.0	0.64	0.77	0.53	4.30	3.3	2.35	1.22	4.00	17.8	2.55
20.0	0.48	0.59	0.40	3.50	2.60	1.84	0.92	3.20	14.3	2.20
30.0	0.32	0.40	0.275	2.55	1.88	1.32	0.63	2.40	10.3	1.75
50.0	0.190	0.245	0.165	1.68	1.27	0.82		1.68	6.75	1.25
70.0	0.135	0.175	0.120	1.28	0.95	0.62		1.30	5.00	0.98
100.0	0.090	0.125	0.085	0.95	0.72	0.44		1.00	3.60	0.76
150.0										0.56
200.0										0.44
300.0										0.32
400.0										0.25

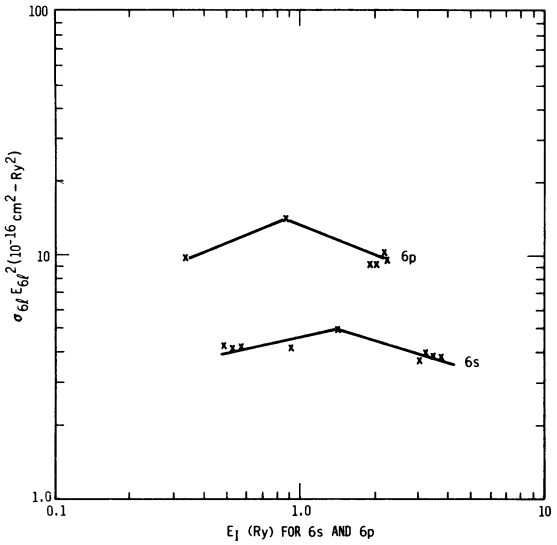

FIG. 15. Calculated $(\sigma_{nl})_{max} E_{nl}^2$ for the $6s$ and $6p$ subshells.

classical scaled $3d$ cross section ($1.3 \leq E_{3d} \leq 50$ Ry) is compared with the measurements of Kojima *et al.* on Cd.[31] The agreement of the reduced measurements and the scaled cross section is good, as the measurements use Auger detection with large background subtractions.

In Fig. 10 the scaled $3d$ cross section in the classical scaling region ($E_{3d} \geq 50$ Ry) is shown along with the reduced measurements of Toburen[15] in Xe, of Busch *et al.*[43] on Pb, and of Ishii *et al.*[44] on Au, Bi, and U. In reducing the data, I used $\omega_{\bar{M}} = 0.023$, 0.030, 0.035, and 0.045, for Au, Pb, Bi, and U. For Au and Bi these are measured values[20]; for U, $\omega_{\bar{M}}$ is that used by Ishii *et al.*[44] and for Pb, $\omega_{\bar{M}}$ is an interpolation from my calculations.[45] For Au, Bi, and U, my calculated or interpolated values are $\omega_{\bar{M}} = 0.026$, 0.032, and 0.047. Bhalla[46] calculated $\omega_{3d} = 0.0281$ and 0.0326 at $Z = 80$ and 83. The calculated and measured $\omega_{\bar{M}}$ are in excellent agreement. The reduced measurements of Toburen,[15] with large error bars, are in agreement with the scaled $3d$ cross section, while the measurements of Ishii *et al.*[44] are in reasonable agreement (less than a factor of 2 difference). The measurements of Busch *et al.*[43] on Pb are considerably higher than the scaled cross section and a factor of 3 higher than the reduced measurements of Ishii *et al.*[44] on the adjacent element Bi. This disagreement between two sets of measurements is similar to that for $2p$ ionization in Ag and Sn, discussed in Sec. IV.

VI. THE SCALED $4s$, $4p$, $4d$, AND $4f$ PROTON IONIZATION CROSS SECTIONS

In Figs. 11 and 12, $(\sigma_{nl})_{max} E_{nl}^2$ is shown versus E_{nl} for the $4s$, $4d$, $4p$, and $4f$ subshells. For the

TABLE VII. Parameters for the scaled $6s$ and $6p$ proton ionization cross sections; $\sigma_{nl}(E_p)(E_{nl})^{\alpha_{nl}} = f_i(M_e E_p / M_p E_{nl})$ with f in units of 10^{-16} cm^2 Ry$^{\alpha}$. The subscripts a and b refer to the following values of α_{nl} and E_{nl}.

	$6s$		$6p$	
	a: $0.50 \leq E_I \leq 1.45$, $\alpha = 1.79$		a: $0.35 \leq E_I \leq 0.85$, $\alpha = 161$	
	b: $1.45 \leq E_I \leq 4.00$, $\alpha = 2.32$		b: $0.85 \leq E_I \leq 2.20$, $\alpha = 2.39$	
η	f_a	f_b	f_a	f_b
0.10		0.13		
0.15		0.64		
0.20		1.33		3.00
0.30	3.00	2.70		5.40
0.50	4.20	4.20	10.6	8.90
0.70	4.60	5.60	13.5	11.2
1.00	4.60	5.70	14.8	13.0
1.50	4.20	5.00	14.6	13.5
2.0	3.60	4.25	13.9	12.8
3.0	2.70	3.15	12.2	10.8
5.0	1.80	2.08	9.4	8.2
7.0	1.35	1.60	7.7	6.7
10.0	0.98	1.15	6.0	5.3
15.0	0.68	0.80	4.5	4.9
20.0	0.52	0.60	3.6	3.10
30.0	0.35	0.41	2.65	2.20
50.0	0.210	0.245	1.75	1.40
70.0	0.146	0.180	1.30	1.03
100.0	0.105	0.125	0.95	0.74

$4d$ and $4f$ subshells, E_{nl} at $Z=102$ is not large enough to reach the classical region. In these two cases the classical cross section was extrapolated to $(\sigma_{4d})_{max}E_{4d}^2 = 5(\sigma_{1s})_{max}E_{1s}^2$ and $(\sigma_{4f})_{max}E_{4f}^2 = 7(\sigma_{1s})_{max}E_{1s}^2$. The scaled cross sections are listed in Tables IV and V.

In Fig. 13 the experimental data on N-shell proton ionization cross sections is compared with the sum of the calculated $4p$- and $4d$-subshell cross sections. The solid curves are the $4p$ and $4p+4d$ cross sections of tungsten, which are compared with the measurements of Tittle and Bell[47] (open circles with error bars). The measurements are significantly lower than the calculations at high energy. The discrepancy is similar to that seen in Toburen's[15] measurements in Xe. The Xe calculation and measurements from Fig. 2, reduced by a factor of 100, are shown as the dashed curve and open squares with error bars. As pointed out in Sec. III, the Xe ($4d$) *electron* ionization cross section, calculated with the same generalized oscillator strengths, is in excellent agreement with experiment.

VII. THE SCALED $5s$, $5p$, $5d$, $5f$, $6s$, AND $6p$ PROTON IONIZATION CROSS SECTIONS

In Fig. 14, $(\sigma_{5l})_{max}E_{5l}^2$ is shown versus E_{5l} for the $5s$, $5p$, $5d$, and $5f$ subshells. The calculations cover a limited range of E_{5l}. The scaled cross sections are listed in Table VI. In Fig. 15, $(\sigma_{6l})_{max}E_{6l}^2$ is shown versus E_{6l} for the $6s$ and $6p$ subshells, and the scaled cross sections are listed in Table VII. Other than the Xe measurements of Toburen,[15] discussed previously, there are no experimental data to compare with the scaled cross sections.

VIII. CONCLUSIONS

The scaled proton ionization cross sections, presented here, are in reasonable agreement with much of the available experimental data. While there are disagreements between some sets of measurement and the calculations for a particular subshell, for other sets of measurements, adjacent elements show excellent agreement with the calculations for the same subshell. Two explanations are (a) that the scaling hypothesis is invalid, or (b) systematic experimental error. The generally good agreement with most measurements suggest that explanation (b) is more probable.

There are few measurements on subshell proton ionization cross sections beyond the M shell. However, electron total ionization cross sections,[6] obtained via scaled subshell cross sections and the same GOS, are in good agreement with measurement in high-Z materials. It is hoped that these calculations will stimulate measurements of proton ionization cross sections for the outer subshells of high-Z elements.

ACKNOWLEDGMENT

This work was supported by the United States Department of Energy.

[1] E. Nardi, E. Peleg, and Z. Zinamon, Phys. Fluids 21, 574 (1978).
[2] Y. Hahn, Phys. Rev. A 18, 1028 (1978).
[3] P. G. Steward and R. W. Wallace, Lawrence Berkeley Report No. UCRL-19428, 1970 (unpublished).
[4] H. A. Bethe, Ann. Phys. (Leipzig) 5, 325 (1930) and Z. Phys. 76, 293 (1932).
[5] E. J. McGuire, Phys. Rev. A 16, 73 (1977).
[6] E. J. McGuire, Phys. Rev. A (in press).
[7] E. J. McGuire, Phys. Rev. A 16, 62 (1977).
[8] F. Herman and S. Skillman, *Atomic Structure Calculations* (Prentice-Hall, Englewood Cliffs, 1963).
[9] E. J. McGuire, Phys. Rev. A 3, 267 (1971).
[10] S. T. Manson, Phys. Rev. A 6, 1013 (1972).
[11] F. J. de Heer, J. Schutten, and H. Moustafa, Physica (Utrecht) 32, 1766 (1966).
[12] H. B. Gilbody and A. R. Lee, Proc. R. Soc. London, Ser A 274, 365 (1963).
[13] R. Hippler and K. H. Schartner, J. Phys. B 7, 1167 (1974).
[14] J. E. Hansen and W. Persson, Phys. Rev. A 18, 1459 (1978).
[15] L. H. Toburen, Phys. Rev. A 9, 2505 (1975).
[16] Th. M. El-Sherbini, M. J. van der Wiel, and F. J. de Heer, Physica (Utrecht) 48, 159 (1970).
[17] C. V. Barros Leite, N. V. de Castro Faria, and A. G. de Pinho, Phys. Rev. A 15, 943 (1977).
[18] Y. K. Kim, M. Inokuti, G. E. Chamberlain, and S. R. Mielczarek, Phys. Rev. Lett. 21, 1146 (1968).
[19] S. T. Manson and A. Msezane, J. Phys. B 8, L5 (1975).
[20] W. Bambynek, B. Crasemann, R. W. Fink, H. W. Freund, H. Mark, C. D. Swift, R. E. Price, and P. V. Rao, Rev. Mod. Phys. 44, 716 (1972).
[21] K. Siegbahn *et al.*, *Electron Spectroscopy for Chemical Analysis* (Almqvist and Wiksells, Stockholm, 1967).
[22] J. M. Khan, D. L. Potter, and R. D. Worley, Phys. Rev. A 139, 1735 (1965).
[23] G. A. Bissinger, J. M. Joyce, E. J. Ludwig, W. S. McEver, and S. M. Shafroth, Phys. Rev. A 1, 841 (1970).
[24] G. A. Bissinger, S. M. Shafroth, and A. W. Waltner, Phys. Rev. A 5, 2046 (1972).
[25] O. N. Jarvis, C. Whitehead, and M. Shah, Phys. Rev. A 5, 1198 (1972).
[26] A. M. Arthurs and B. L. Moiseiwitsch, Proc. R. Soc. London, Ser. A 247, 550 (1958).
[27] R. Akselsson and T. B. Johannson, Z. Phys. 266,

245 (1974).
[28]L. M. Winters, J. R. MacDonald, M. D. Brown, L. D. Ellsworth, and T. Chiao, Phys. Rev. A 7, 1276 (1973).
[29]T. K. Li, D. L. Clark, and G. W. Greenlees, Phys. Rev. A 14, 2016 (1976).
[30]N. Stolterfoht, D. Schneider, and P. Ziem, Phys. Rev. A 10, 81 (1974).
[31]H. Kojima, N. Kobayashi, N. Maeda, and M. Sakisaka, J. Phys. Soc. Jpn. 46, 198 (1979).
[32]N. Maeda, N. Kobayashi, H. Hori, and M. Sakisaka, J. Phys. Soc. Jpn. 40, 1430 (1976).
[33]A. Langenberg, F. J. de Heer, and J. VanEck, J. Phys. B 8, 2079 (1975).
[34]F. Bertrand, G. Charpak, and F. Suzor, J. Phys. Radium 20, 462 (1959); 20, 956 (1959).
[35]L. E. Bailey and J. B. Swedlund, Phys. Rev. 158, 6 (1967).
[36]M. H. Chen, B. Crasemann, and V. O. Kostroun, Phys. Rev. A 4, 1 (1971).
[37]E. J. McGuire, Phys. Rev. A 3, 587 (1971).
[38]D. L. Walters and C. P. Bhalla, Phys. Rev. A 4, 2164 (1971).
[39]R. P. Chaturvedi, R. M. Wheeler, R. B. Liebert, D. J. Mijanic, T. Zabel, and G. C. Phillips, Phys. Rev. A 12, 52 (1975).
[40]M. R. Khan, A. G. Hopkins, and D. Crumpton, Z. Phys. A 288, 133 (1978).
[41]K. Ishii, S. Morita, H. Tawara, H. Kaji, and T. Shiokawa, Phys. Rev. A 10, 774 (1974).
[42]B. H. Choi, Phys. Rev. A 11, 2004 (1975).
[43]C. E. Busch, A. B. Baskin, P. H. Nettles, and S. M. Shafroth, Phys. Rev. A 7, 1601 (1973).
[44]K. Ishii, S. Morita, H. Tawara, H. Kaji, and T. Shiokawa, Phys. Rev. A 11, 119 (1975).
[45]E. J. McGuire, Phys. Rev. A 5, 1043 (1972); and in *Proceedings of the International Conference on Inner Shell Ionization Phenomena and Future Applications*, edited by R. W. Fink, S. T. Manson, J. M. Palms, and P. V. Rao (AEC, Oak Ridge, Tenn., 1973).
[46]C. P. Bhalla, Phys. Rev. A 6, 1409 (1972).
[47]H. Tittel and F. Bell, Z. Phys. A 287, 143 (1978).